Electrochimica Acta 111 (2013) 165–171

Contents lists available at ScienceDirect

Electrochimica Acta

journal homepage: www.elsevier.com/locate/electacta

# Coaxial MWNTs@$MnO_2$ confined in conducting PPy for kinetically efficient and long-term lithium ion storage☆

Jiaxin Li[a,b], Mingzhong Zou[a], Yi Zhao[b], Yingbin Lin[a], Heng Lai[a], Lunhui Guan[b], Zhigao Huang[a,*]

[a] College of Physics and Energy, Fujian Normal University, Fuzhou 350007, China
[b] Fujian Institute of Research on the Structure of Matter, Chinese Academy of Sciences, Fuzhou 350002, China

ARTICLE INFO

*Article history:*
Received 25 April 2013
Received in revised form 2 July 2013
Accepted 30 July 2013
Available online xxx

*Keywords:*
MWNTs@$MnO_2$@PPy composites
Rate performance
Equivalent circuit
Anode materials

ABSTRACT

Coaxial MWNTs@$MnO_2$ confined in conducting polypyrrole (PPy) has been synthesized through an in situ polymerization of pyrrole monomers in the presence of prepared MWNTs@$MnO_2$. As an anode in lithium batteries (LIBs), the obtained MWNTs@$MnO_2$@PPy shows a high reversible capacity of 530 mA h $g^{-1}$ tested at 1000 mA $g^{-1}$ even after 300 cycles and an excellent rate performance. The superior electrochemical performance of the nanocable MWNTs@$MnO_2$@PPy is associated with a synergistic effect of the MWNT matrix and the highly conducting PPy coating layer. This nanocable configuration not only facilitates electron conduction but also maintains the structural integrity of active materials. In addition, an analysis of the AC impedance spectroscopy and the corresponding hypothesis for DC impedance confirm that such configuration can effectively enhance the charge-transfer efficiency and the lithium diffusion coefficient. Thus, PPy modification supplied a promising route to obtain manganese oxide based anode in order to achieve high-performance LIBs.



## 1. Introduction

With the rapid increase of energy consumption of portable electronic device and hybrid electric vehicles, it is highly desirable to develop high capacity and high energy density LIBs [1–3]. Though commercial graphite with a theoretical capacity of 372 mA h $g^{-1}$ has been developed with improved performance, its power density for LIBs is still too low to meet the increasingly growing demand for high-level applications. Recently, manganese oxide ($MnO_x$), especially for layer structure $MnO_2$ consisted of 2D edge-shared [$MnO_6$] octahedra layers with $K^+$ cations and water molecules in the interlayer, beneficial for $Li^+$ transfer, has been believed to be a promising anode material for LIBs, owing also to its low cost, environmental friendliness, natural abundance and high storage capacity (1230 mA h $g^{-1}$) [3–8]. However, the drawbacks such as large volume expansion during repeated lithium cycling processes and intrinsically poor electrical conductivity can lead to rapid deterioration of the electrode, thus greatly limiting the practical use of the $MnO_2$ anode materials [5,9–13]. Many useful strategies have been proposed to overcome these issues. For instance, the preparation of $MnO_2$ nanostructures, such as spheres [9], nanowires [10], nanotubes [11,12], nanoflakes [5,13], and nanoplatelets [14], has attracted extensive attention. Besides the above-mentioned synthesis strategies, researchers focused on using carbonaceous materials (CMs) including carbon nanotubes [6,12], carbon nanohorns [15] and graphene [16,17] as buffer carriers for suppressing the pulverization and capacity fading of $MnO_2$ anodes to some extent. In short, various nanostructures can only give a limited improvement in the electrochemical performance of $MnO_2$, but generally at lower rates (0.1–0.5 C), whereas at higher rates capacity and cycling life are not satisfactory. For $MnO_2$/CM composites, the connection between $MnO_2$ and CMs is usually weak, which still gives rise to large volume change during cycling process. So, it is still a significant challenge to develop an appropriate method for achieving its high performance.

Recently, using conductive polymers to improve electrochemical performance of electrode materials for LIBs has attracted extensive attention [18–20]. Herein, the well-known polypyrrole (PPy) has been applied in lithium storage materials, due to their good intrinsic electrical conductivity ($10^2$–$10^3$ S/cm) and chemical stability [19,21]. Moreover, the PPy matrix also shows the function of accommodating the internal stress of electrode materials that suffer from severe volume change. Recently, Chen [20] et al.



* Corresponding author. Tel.: +86 591 22867577; fax: +86 591 22867577.
*E-mail addresses:* guanlh@fjirsm.ac.cn (L. Guan), zghuang@fjnu.edu.cn, ljx@fjirsm.ac.cn (Z. Huang).

0013-4686/$ – see front matter © 2013 The Authors. Published by Elsevier Ltd. All rights reserved.
http://dx.doi.org/10.1016/j.electacta.2013.07.224

modified nanosize $SnO_2$ with soft PPy matrix to form a conducting polymer/$SnO_2$ composite anode and effectively improved its electrochemical performance. The similar reports revealed that the PPy coating on Sn [22], SWNTs@$SnO_2$[23], MWNTs@$SnO_2$ [24], CuO [25], and $V_2O_5$ [26] would possess favorable electrochemical properties. But up to now, to the best of our knowledge, using PPy to coat on MWNTs@$MnO_2$ anode has not been reported.

In this study, we attempt to introduce PPy to uniformly coat on the surface of MWNTs@$MnO_2$ via using the chemical oxidation polymerization method and form a homogeneous organic-inorganic hybrid material, MWNTs@$MnO_2$@PPy, with the aim of improving its electrochemical performance for LIBs. The structure, morphology and electrochemical properties of these nanocomposites were investigated systematically. Compared with the MWNTs@$MnO_2$, the MWNTs@$MnO_2$@PPy anode exhibited an obviously better electrochemical performance including reversible capacity, cycling performance, and rate performance. It delivered a high capacity of 530 mA h $g^{-1}$ tested at 1000 mA $g^{-1}$ even after 300 cycles. In addition, new insights on the impedance analysis for enhanced mechanism are provided.

## 2. Experimental

### 2.1. Materials synthesis

Experimentally, all chemicals were of analytical grade. The MWNTs were purchased from Shenzhen Nanotech Port (Shenzhen, China) and used as received. The mechanism for the synthesis of the MWNTs@$MnO_2$ composite is described in our previous work [27]. $MnO_2$ nanoflakes loading on MWNTs were synthesized by immersing MWNTs into a $KMnO_4$ aqueous solution. Briefly, the reaction mechanism in acidic solution between MWNTs and $KMnO_4$ can be proposed as the equation of "$4MnO_4^- + 3C + 4H^+ \rightarrow 4MnO_2 + 3CO_2 + 2H_2O$". 100 mg $KMnO_4$ was dispersed in 50 ml de-ionized water and heated to 80 °C. And 100 mg MWNTs were added to the solution and the mixtures were maintained at 80 °C for 10 h. The pH of the solution was adjusted to 3.0 by adding 2 M HCl. The product was filtered and washed by de-ionized water, and then dried at 100 °C overnight.

In a typical experiment, 50 mg MWNTs@ $MnO_2$ composite was first sonicated in 30 mL of deionized water containing 4 mg of sodium lauryl sulfate (SDS) for 20 min and stirred magnetically for 1 h. Then, 21.0 μL of pyrrole was added and stirring continued for 1 h. Finally, 6 mL of 0.1 M ammonium persulfate aqueous solution was slowly dropped into the above solution. The polymerization process was kept under stirring for 4 h in an ice-water bath. The final composite was filtered, washed with deionized water and ethanol several times, and then dried at 80 °C overnight. The process is briefly shown in Scheme 1.

### 2.2. Materials characterization

The structure and morphology of the composites were characterized by X-ray diffraction (XRD, RIGAKU SCXmini), ourier transform infrared spectroscopy (FTIR), scanning electron microscope (SEM, JSM-6700F), thermal gravimetric analysis (TGA, NETZSCH STA449 C) and transmission electron microscope (TEM, Tecnai G2 F20). TGA tests were measured from 30 to 1000 °C at a heating rate of 10 K $min^{-1}$ in air, to evaluate the weight content of $MnO_2$ in these hybrid materials.

### 2.3. Electrochemical measurements

The electrochemical behaviors were measured via CR2025 cointype test cells assembled in a dry argon-filled glove box. The test cell consisted of working electrode (~1.5 mg $cm^{-2}$) and lithium sheet

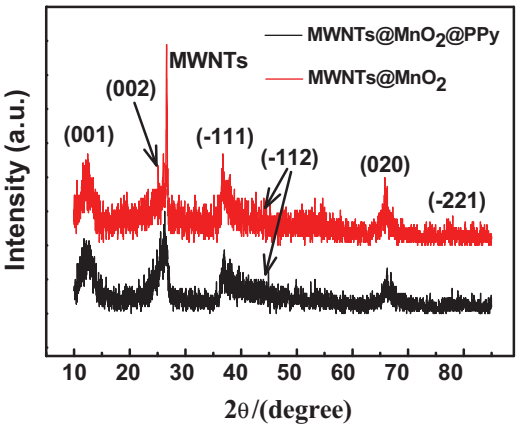


**Fig. 1.** XRD patterns of the MWNTs@$MnO_2$ and MWNTs@$MnO_2$@PPy.

which were separated by a Celgard 2300 membrane and electrolyte of 1 M LiPF6 in EC:EMC:DMC (1:1:1 in volume). The working electrode consisted of 80 wt.% active material, 10 wt.% carbon black and 10 wt.% polymer binder (Carboxymethyl cellulose, Na-CMC). The electrodes were dried at 100 °C for 12 h in a vacuum. Cyclic voltammetry tests were operated on a CHI660D Electrochemical Workstation with a scan rate of 0.50 mV $s^{-1}$. The cells were cycled by LAND 2001A at room temperature. Electrochemical impedance measurements were carried out by applying an ac voltage of 5 mV over the frequency range from 1 mHz to 100 kHz. In addition, the specific capacities in this article were calculated based on the overall mass of the composite.

## 3. Results and discussion

The crystalline structure of the MWNTs@$MnO_2$ and MWNTs@$MnO_2$@PPy was investigated by XRD. From Fig. 1, the diffraction peaks at 12.5°, 25.2°, 37.3°, 42.5°, 65.6° and 79.9° presented both in MWNTs@$MnO_2$ and MWNTs@$MnO_2$@PPy can be well-assigned to the (0 0 1), (0 0 2), (−1 1 1), (−1 1 2), (0 2 0) and (−2 2 1) planes of $MnO_2$ crystal according to the standard data file (JCPDS no. 80-1098). The diffraction peak of MWNTs near 26.5° was overlapped with the (0 0 2) plane of the $MnO_2$ in the composites. MWNTs@$MnO_2$@PPy show an XRD pattern similar to that of MWNTs@$MnO_2$ but the peak at 26° for MWNTs has slightly weakened, suggesting the crystal structure of $MnO_2$ is not affected. Furthermore, the corresponding selected area electron diffraction patterns (Fig. S1) also corroborate the polycrystallinity of these two samples, which are in agreement with the XRD results.

The morphology and structure of the samples were first examined by scanning electron microscope (SEM) and transmission electron microscope (TEM). As shown in Fig. 2a, the as-obtained MWNTs@$MnO_2$ shows homogeneous cross-linked morphology with diameter in the range 50–70 nm. After PPy coating, the MWNTs@$MnO_2$ becomes a little thicker with size increased to approximately 70–90 nm (Fig. 2b), indicating that the thickness of the PPy layer is about ~10 nm. It should be noted that none of the PPy layer blocked the opening of the three-dimensional entangled structure of the MWNTs@$MnO_2$. The same results can also be found in the TEM images shown in Fig. 2c and d. In addition, the clear interlayer spacing of 0.21, 0.24 and 0.70 nm, corresponding to the (−1 1 2), (−1 1 1) and (0 0 1) planes of $MnO_2$, could be found in the HRTEM image (insets of Fig. 2c and d). For MWNTs@$MnO_2$@PPy, the TEM image also shows that the PPy is well coated on the surface of the MWNTs@$MnO_2$ (inset of Fig. 2c). The uniform PPy coating is beneficial to the fast diffusion and migration of ions in the polymer, thereby improving the electrochemical performance of electrode.

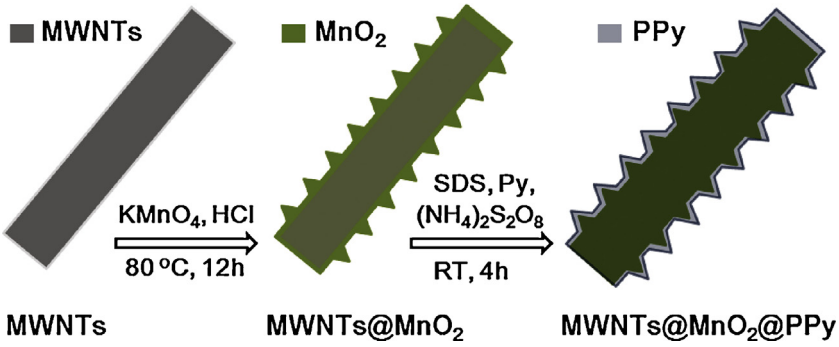


**Scheme 1.** Schematic illustration of the fabrication of MWNTs@$MnO_2$@PPy using a two-step approach.

In order to further confirm the presence of PPy, element mapping was used to observe the distribution of PPy. As presented in Fig. 3, the color points are due to the presence of the element. The element N is present due to the presence of PPy. It can be seen that C, O, Mn and N in the sample are homogeneously distributed in the composite, indicating the conducting PPy is homogenously coated on the surface of the MWNTs@$MnO_2$. Furthermore, the FTIR spectra presented in Fig. S2 are also used to verify the chemical structure of MWNTs@$MnO_2$@PPy. The FTIR data provide another proof to confirm the presence of PPy on the surface of MWNTs@$MnO_2$. Based on the TGA result in Fig. S3, the loading ratio of $MnO_2$ in MWNTs@$MnO_2$ composite is 48 wt.%, and that of PPy in the MWNTs@$MnO_2$@PPy composite was about 16 wt.%.

To evaluate the electrochemical behavior, coin cells based on MWNTs@$MnO_2$ and MWNTs@$MnO_2$@PPy composites were subjected to cyclic voltammetry (CV) testing as well as discharge–charge (D-C) cycling. Fig. 4a shows the initial seven CV curves of the MWNTs@$MnO_2$ composite at a scan of 0.5 mV $s^{-1}$ with a cutoff window of 0.05–3.00 V. There was a broad reduction peak near 2.5 V in the 1st cathodic scan, which was attributed to the decomposed electrolyte. A following irreversible reduction peak of 0.60 V is assigned to the formation of a solid electrolyte interface (SEI) layer and the reduction of $Mn^{4+}$ to $Mn^{2+}$, while the intense peak from 0.25 to 0.05 V can be ascribed to the further reduction of $Mn^{2+}$ to metallic Mn and the Li ions intercalate in MWNTs. Two oxidation peaks at 1.30 and 2.30 V in the 1st anodic scan can be observed, which means that the electrochemical oxidation

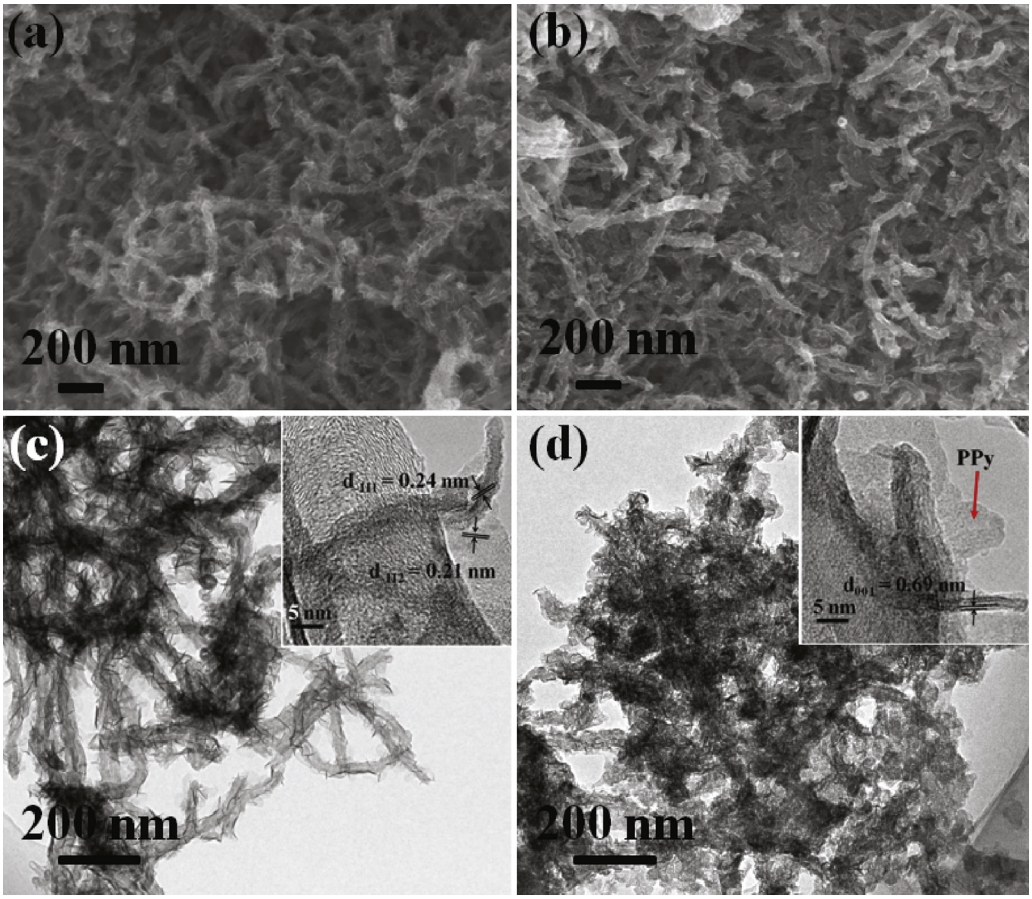


**Fig. 2.** (a) and (b) SEM images of the MWNTs@$MnO_2$ and MWNTs@$MnO_2$@PPy; (c) and (d) TEM and the corresponding HR-TEM images of the MWNTs@$MnO_2$ and MWNTs@$MnO_2$@PPy.

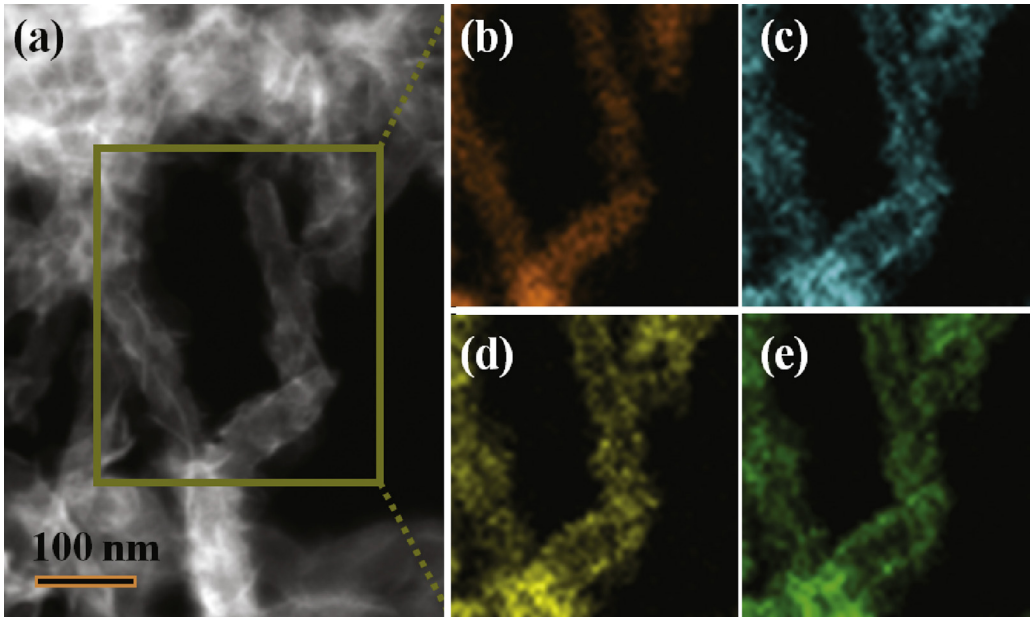


**Fig. 3.** STEM image (a) and carbon (b), oxygen (c), manganese (d), nitrogen (e) element mapping images of as-obtained MWNTs@$MnO_2$@PPy.

reaction proceeds by two steps. From the 2nd cycle, the repeated Li ions insertion/extraction in/out MWNTs@$MnO_2$ leads to two pairs of redox peaks at ~0.2/1.3 V and ~1.0/2.3 V, respectively. Compared with MWNTs@$MnO_2$, Fig. 4b shows that the redox peaks of the 7th cycle is very close to the 2nd one, which exhibits good reproducibility and similar shapes, revealing a better electrochemical stability for MWNTs@$MnO_2$@PPy anode. In addition, the 0.55 V reduction peaks presented in both samples disappear in the subsequent cycles, indicating that formation of the SEI layer only takes place during the 1st cycle. Accordingly, the first two D-C voltage profiles of these two electrodes are shown in Fig. 4c and d. The related potential plateaus such as 0.55, 1.30 and 2.30 V in the D-C process are consistent with the results of CVs.

The cycling performance for MWNTs@$MnO_2$ and MWNTs@$MnO_2$@PPy electrodes in the voltage range 0.05–3.0 V is displayed in Fig. 5. Fig. 5a compares the cycling performance of these two composites at 100 mA $g^{-1}$. Apparently, the MWNTs@$MnO_2$@PPy electrode exhibited a significantly improved

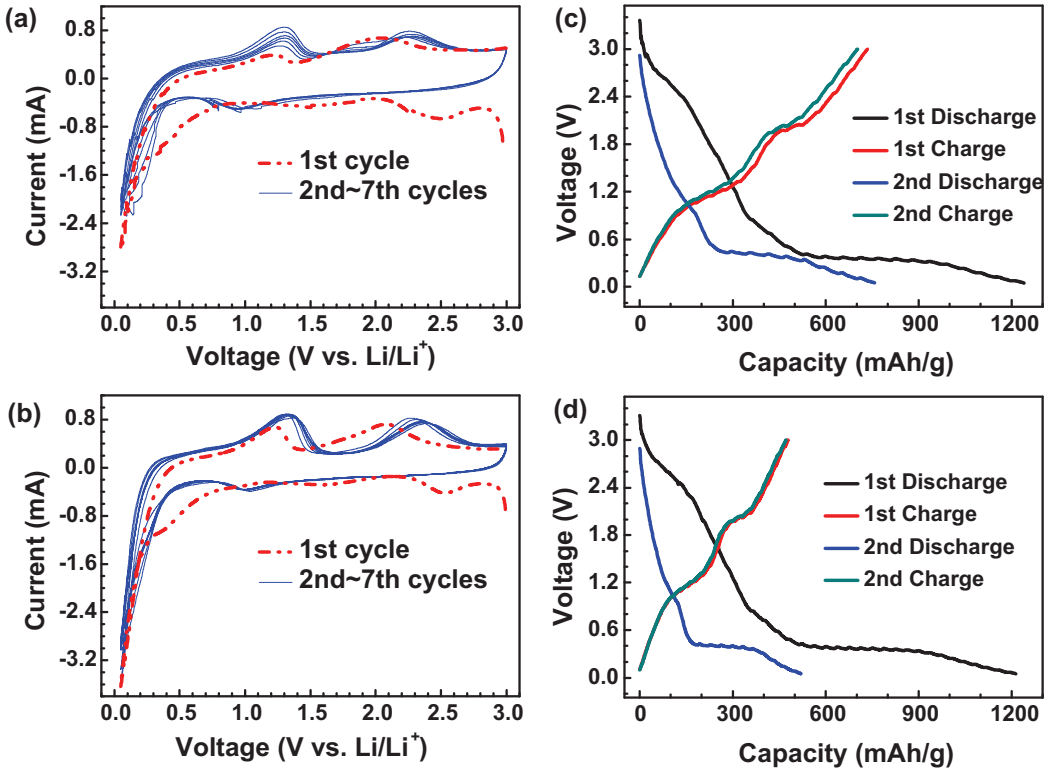


**Fig. 4.** Cyclic voltammetry curves and first two discharge–charge curves between 0.05 and 3 V (versus $Li/Li^+$) of Li insertion/extraction into/from two electrodes: (a, c) MWNTs@$MnO_2$ and (b, d) MWNTs@$MnO_2$@PPy.

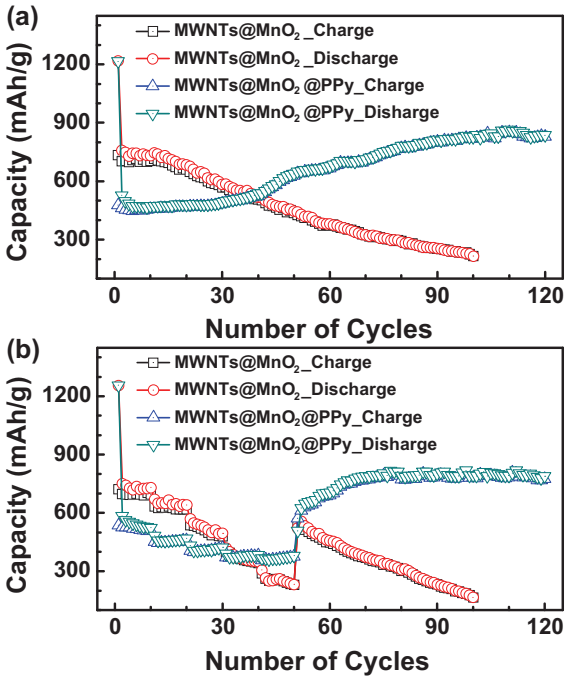


**Fig. 5.** Cycling performance of MWNTs@$MnO_2$ and MWNTs@$MnO_2$@PPy electrodes: (a) at a current density of 100 mA $g^{-1}$; (b) at various current rates of 100, 200, 400, 800, 1000 and 100 mA $g^{-1}$, respectively.

cyclic capacity. The reversible capacity for the MWNTs@$MnO_2$@PPy electrode retains at ~450 mA h $g^{-1}$ after 30 cycles, and then increases with cycling and reaches ~820 mA $g^{-1}$ after 120 cycles. It should be pointed out that the coulombic efficiency for MWNTs@$MnO_2$@PPy increases quickly to 100% after a few cycles. However, the MWNTs@$MnO_2$ only delivered a low capacity of ~200 mA h $g^{-1}$ after 100 cycles. In addition to high capacity and good electrochemical stability, the rate performance of MWNTs@$MnO_2$@PPy was also tested by changing the current density. As presented in Fig. 5b, the specific capacities of MWNTs@$MnO_2$@PPy were 530, 450, 400, 370, 350 mA h $g^{-1}$ when cycled under the current densities of 100, 200, 400, 800 and 1000 mA $g^{-1}$, respectively. When the current density is turned back to 100 mA $g^{-1}$ after 50 cycles at various rates, the capacity can recover to 800 mA h $g^{-1}$ and retain for even 120 cycles. In contrast, the capacities for MWNTs@$MnO_2$ cycled at different rates progressively decreased with cycling and only delivered a low capacity of ~180 mA h $g^{-1}$ after 100 cycles.

We further evaluated the long cycle performance of the MWNTs@$MnO_2$@PPy anode at relatively high current densities of 500 and 1000 mA $g^{-1}$ after being activated at 100 mA $g^{-1}$ in the first three cycles. As presented in Fig. 6, the specific reversible capacity measured at 1000 mA $g^{-1}$ can still stabilize at 530 mA h $g^{-1}$ after 300 cycles. As discussed later, the excellent lithium storage performance should be promoted by the MWNT supporter and uniform PPy coating.

As we know, electrochemical impedance spectroscopy (EIS) is a highly resolved electro-analytical technique that may provide unique information about the nature of electrode process related to a wide range of time constants [28]. Fig. 7 presents EIS profiles of MWNTs@$MnO_2$ and MWNTs@$MnO_2$@PPy after test and the corresponding equivalent circuit. The overall shape of Nyquist plots for all samples are composed of three parts, essentially two semicircles followed by a one line. According to the literature [20,26], the high-frequency semicircle is related to Li ion migration through the SEI film covering the surface of the electrode, the middle-frequency semicircle is attributed to charge transfer

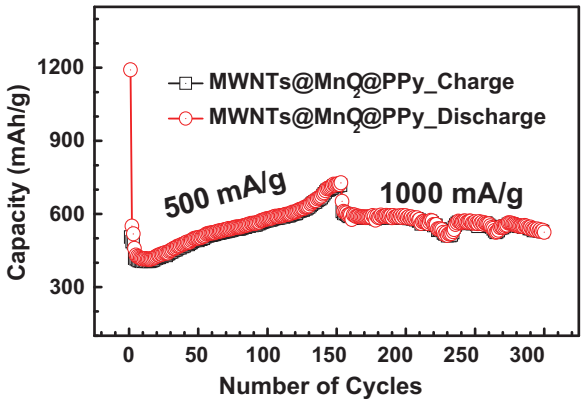


**Fig. 6.** Long cycle performance of MWNTs@$MnO_2$@PPy electrode.

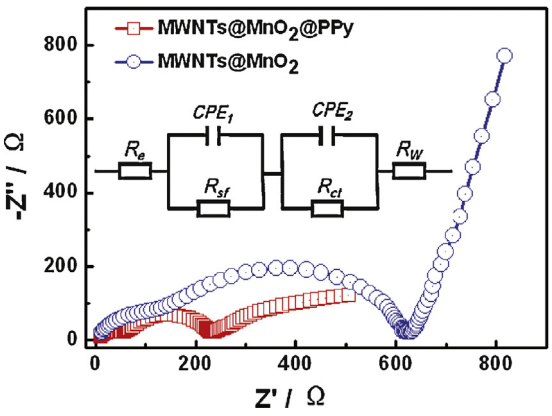


**Fig. 7.** The EIS profiles of MWNTs@$MnO_2$ and MWNTs@$MnO_2$@PPy anodes after long cycling. The inset shows the corresponding equivalent circuit.

through the electrode/electrolyte interface, and the steep sloping line is assigned to solid-state diffusion of the Li ions into the bulk of the electrode material. The impedance spectra are fitted with an equivalent circuit as shown in the inset of Fig. 7, where the symbols, $R_e$, $R_{sf}$, $R_{ct}$, and $R_w$, denote the solution resistance, the diffusion resistance of Li ions through SEI layer, the charge-transfer resistance and Warburg impedance, respectively. As shown in Table 1, the fitting results of $R_e$, $R_{sf}$, $R_{ct}$, and $R_w$ of both samples indicate that the $R_{ct}$ value of PPy coating composite is smaller than that of MWNTs@$MnO_2$, indicating that the presence of PPy can significantly improve the charge transfer resistance for electrode. To further investigate the electrode kinetics, the diffusion coefficient of Li ions ($D_{Li}^+$) can be calculated from EIS data via a previously reported method [29]. Fig. S4 shows the linear fitting of $Z_{real}$ vs. $\omega^{-1/2}$, from which the slope $\sigma$ can be obtained. The related calculation was also shown in supplementary information. The $D_{Li}^+$ for MWNTs@$MnO_2$@PPy is calculated to be $8.7 \times 10^{-11}$ $cm^2$ $S^{-1}$. In comparison, that of MWNTs@$MnO_2$ shows a lower value of $1.1 \times 10^{-11}$ $cm^2$ $S^{-1}$. The result should be attributed to the unique nanostructure of MWNTs@$MnO_2$@PPy, in which the porous and conductive PPy matrix serves as efficient diffusion channels for Li ions.

**Table 1**
Impedance parameters of MWNTs@$MnO_2$ and MWNTs@$MnO_2$@PPy anodes after test.

| | $R_e$ (Ω) | $R_{sf}$ (Ω) | $R_{ct}$ (Ω) | $D_{Li}^+$ ($cm^2$ $S^{-1}$) |
|---|---|---|---|---|
| MWNTs@$MnO_2$ | 9.9 | 128.6 | 423.5 | $1.1 \times 10^{-11}$ |
| MWNTs@$MnO_2$@PPy | 8.4 | 132.9 | 52.2 | $8.7 \times 10^{-11}$ |

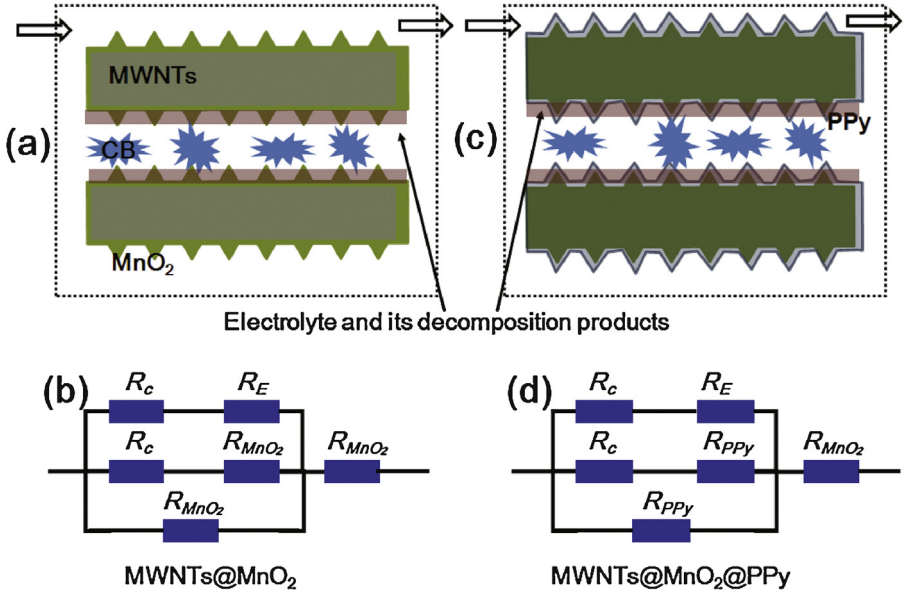


**Fig. 8.** The phenomenological resistance models and corresponding equivalent circuits for (a, b) MWNTs@$MnO_2$ and (c, d) MWNTs@$MnO_2$@PPy.

For practical application, the electrochemical mechanism under direct-current (DC) mode for these coin cells should be carried out. In addition, the degradation of the conductivity in electrode can result in an enhanced interface polarization, which is considered to be responsible for the deterioration of the electrochemical performance. According to scattering theory of electron transport across the interface [30], phenomenological resistance models are set up and the corresponding DC equivalent circuits between active materials describing these processes are shown in Fig. 8, which includes the carbon (MWNTs and CB) resistance $R_c$, the $MnO_2$ resistance $R_{MnO_2}$, the PPy resistance $R_{PPy}$, and the $R_e$ for surface resistance arising from the species on the anode surface, respectively. Compared these two samples shown in Fig. 8c and d, the total resistance of MWNTs@$MnO_2$@PPy in parallel is much smaller than the pristine one. Thus, the presence of high electronic-conductive PPy on the surface of the anode is beneficial to reduce the total resistance. As a result, the cycling stability can be improved with PPy coating. Fig. S5 reveals that the improved electrochemical performance of MWNTs@$MnO_2$@PPy is also due to the stabilization of the nanocable structure.

## 4. Conclusion

In summary, a nanocable $MnO_2$@MWNT@PPy is developed for use as an excellent performance anode in LIBs. It was prepared through an in situ polymerization of pyrrole monomers in the presence of prepared MWNTs@$MnO_2$. Benefiting from the synergistic effect of the MWNT matrix and the conducting PPy coating layer, the MWNTs@$MnO_2$@PPy electrode displays a high capacity, superior cyclic stability and excellent rate performance. These results indicate the great potential of PPy coating manganese oxide based anode for high-performance lithium batteries.

## Acknowledgements

We acknowledge the financial support by the Natural Science Foundations of China (No. 21203025, No. 51202031, No. 11004032 and No. 11074039).Supplementary data

Supplementary data associated with this article can be found, in the online version, at http://dx.doi.org/10.1016/j.electacta.2013.07.224.

## References

[1] B. Scrosati, J. Hassoun, Y.-K. Sun, Lithium-ion batteries: a look into the future, Energy Environ. Sci. 4 (2011) 3287.
[2] L. Lu, X. Han, J. Li, J. Hua, M. Ouyang, A review on the key issues for lithium-ion battery management in electric vehicles, J. Power Sources 226 (2013) 272–288.
[3] W. Wei, X. Cui, W. Chen, D.G. Ivey, Manganese oxide-based materials as electrochemical supercapacitor electrodes, Chem. Soc. Rev. 40 (2011) 1697–1721.
[4] X. Fang, X. Lu, X. Guo, Y. Mao, Y.-S. Hu, J. Wang, Z. Wang, F. Wu, H. Liu, L. Chen, Electrode reactions of manganese oxides for secondary lithium batteries, Electrochem. Commun. 12 (2010) 1520–1523.
[5] L. Xing, C. Cui, C. Ma, X. Xue, Facile synthesis of α-$MnO_2$/graphene nanocomposites and their high performance as lithium-ion battery anode, Mater. Lett. 65 (2011) 2104–2106.
[6] H. Wang, L.-F. Cui, Y. Yang, H. Sanchez Casalongue, J.T. Robinson, Y. Liang, Y. Cui, H. Dai, $Mn_3O_4$–graphene hybrid as a high-capacity anode material for lithium ion batteries, J. Am. Chem. Soc. 132 (2010) 13978–13980.
[7] X. Li, D. Li, L. Qiao, X. Wang, X. Sun, P. Wang, D. He, Interconnected porous MnO nanoflakes for high-performance lithium ion battery anodes, J. Mater. Chem. 22 (2012) 9189–9194.
[8] K. Zhang, P. Han, L. Gu, L. Zhang, Z. Liu, Q. Kong, C. Zhang, S. Dong, Z. Zhang, J. Yao, H. Xu, G. Cui, L. Chen, Synthesis of nitrogen-doped MnO/Graphene nanosheets hybrid material for lithium ion batteries, ACS Appl. Mater. Interfaces 4 (2012) 658–664.
[9] J. Zhao, Z. Tao, J. Liang, J. Chen, Facile synthesis of nanoporous γ-$MnO_2$ structures and their application in rechargeable li-ion batteries, Crystal Growth Design 8 (2008) 2799–2805.
[10] D.H. Park, S.H. Lee, T.W. Kim, S.T. Lim, S.J. Hwang, Y.S. Yoon, Y.H. Lee, J.H. Choy, Non-hydrothermal synthesis of 1D nanostructured manganese-based oxides: effect of cation substitution on the electrochemical performance of nanowires, Adv. Funct. Mater. 17 (2007) 2949–2956.
[11] L. Li, C. Nan, J. Lu, Q. Peng, Y. Li, Alpha-$MnO_2$ nanotubes: high surface area and enhanced lithium battery properties, Chem. Commun. (Camb) 48 (2012) 6945–6947.
[12] A.L.M. Reddy, M.M. Shaijumon, S.R. Gowda, P.M. Ajayan, Coaxial $MnO_2$/carbon nanotube array electrodes for high-performance lithium batteries, Nano Lett. 9 (2009) 1002–1006.
[13] H. Xia, M. Lai, L. Lu, Nanoflaky $MnO_2$/carbon nanotube nanocomposites as anode materials for lithium-ion batteries, J. Mater. Chem. 20 (2010) 6896–6902.
[14] X. Li, H. Song, H. Wang, Y. Zhang, K. Du, H. Li, J. Huang, A nanocomposite of graphene/$MnO_2$ nanoplatelets for high-capacity lithium storage, J. Appl. Electrochem. 42 (2012) 1065–1070.
[15] H. Lai, J. Li, Z. Chen, Z. Huang, Carbon nanohorns as a high-performance carrier for $MnO_2$ anode in lithium-ion batteries, ACS Appl. Mater. Interfaces 4 (2012) 2325–2328.
[16] C.X. Guo, M. Wang, T. Chen, X.W. Lou, C.M. Li, A hierarchically nanostructured composite of $MnO_2$/conjugated polymer/graphene for high-performance lithium ion batteries, Adv. Eng. Mater. 1 (2011) 736–741.
[17] A. Yu, H.W. Park, A. Davies, D.C. Higgins, Z. Chen, X. Xiao, Free-standing layer-by-layer hybrid thin film of graphene-$MnO_2$ nanotube as anode for lithium ion batteries, J. Phys. Chem. Lett. 2 (2011) 1855–1860.

[18] Z. Dong, S.J. Kennedy, Y. Wu, Electrospinning materials for energy-related applications and devices, J. Power Sources 196 (2011) 4886–4904.
[19] Y.-C. Liu, B.-J. Hwang, Enhancement of conductivity stability of polypyrrole films modified by valence copper and polyethylene oxide in an oxygen atmosphere, Thin Solid Films 360 (2000) 1–9.
[20] L. Cui, J. Shen, F. Cheng, Z. Tao, J. Chen, $SnO_2$ nanoparticles@polypyrrole nanowires composite as anode materials for rechargeable lithium-ion batteries, J. Power Sources 196 (2011) 2195–2201.
[21] P. Si, S. Ding, X.-W. Lou, D.-H. Kim, An electrochemically formed three-dimensional structure of polypyrrole/graphene nanoplatelets for high-performance supercapacitors, RSC Adv. 1 (2011) 1271.
[22] S.L. Chou, X.W. Gao, J.Z. Wang, D. Wexler, Z.X. Wang, L.Q. Chen, H.K. Liu, Tin/polypyrrole composite anode using sodium carboxymethyl cellulose binder for lithium-ion batteries, Dalton Trans. 40 (2011) 12801–12807.
[23] Y. Zhao, J. Li, N. Wang, C. Wu, G. Dong, L. Guan, Fully reversible conversion between $SnO_2$ and Sn in SWNTs@$SnO_2$@PPy coaxial nanocable as high performance anode material for lithium ion batteries, J. Phys. Chem. C 116 (2012) 18612–18617.
[24] Q.-G. Shao, W.-M. Chen, Z.-H. Wang, L. Qie, L.-X. Yuan, W.-X. Zhang, X.-L. Hu, Y.-H. Huang, $SnO_2$-based composite coaxial nanocables with multi-walled carbon nanotube and polypyrrole as anode materials for lithium-ion batteries, Electrochem. Commun. 13 (2011) 1431–1434.
[25] Z. Yin, Y. Ding, Q. Zheng, L. Guan, CuO/polypyrrole core–shell nanocomposites as anode materials for lithium-ion batteries, Electrochem. Commun. 20 (2012) 40–43.
[26] C.-J. Cui, G.-M. Wu, H.-Y. Yang, S.-F. She, J. Shen, B. Zhou, Z.-H. Zhang, A new high-performance cathode material for rechargeable lithium-ion batteries: Polypyrrole/vanadium oxide nanotubes, Electrochim. Acta 55 (2010) 8870–8875.
[27] J. Li, N. Wang, Y. Zhao, Y. Ding, L. Guan, $MnO_2$ nanoflakes coated on multi-walled carbon nanotubes for rechargeable lithium-air batteries, Electrochem. Commun. 13 (2011) 698–700.
[28] S.-D. Xu, Q.-C. Zhuang, L.-L. Tian, Y.-P. Qin, L. Fang, S.-G. Sun, Impedance spectra of nonhomogeneous, multilayered porous composite graphite electrodes for li-ion batteries: experimental and theoretical studies, J. Phys. Chem. C 115 (2011) 9210–9219.
[29] Y. Lin, Y. Lin, T. Zhou, G. Zhao, Y. Huang, Y. Yang, Z. Huang, Electrochemical performance of $LiFePO_4$/Si composites as cathode material for lithium ion batteries, Mater. Chem. Phys. 138 (2013) 313–318.
[30] Z. Huang, Z. Chen, K. Peng, D. Wang, F. Zhang, W. Zhang, Y. Du, Monte Carlo simulation of tunneling magnetoresistance in nanostructured materials, Phys. Rev. B 69 (2004) 094420.